

# Evaluation of lymphatic flow pattern using indocyanine green fluorescence imaging in a highly metastatic mouse model

Masashi Yamamoto<sup>1</sup>  | Kohei Taniguchi<sup>1,2</sup>  | Tomo Tominaga<sup>1</sup> | Masa-Aki Shibata<sup>3</sup>  |  
Yosuke Inomata<sup>1</sup> | Kazumasa Komura<sup>2</sup>  | Wataru Osumi<sup>1</sup> | Hiroki Hamamoto<sup>1</sup> |  
Keitaro Tanaka<sup>1</sup> | Junji Okuda<sup>1</sup> | Kazuhisa Uchiyama<sup>1</sup>

<sup>1</sup>Departments of General and Gastroenterological Surgery, Osaka Medical College, Takatsuki, Japan

<sup>2</sup>Translational Research Program, Osaka Medical College, Takatsuki, Japan

<sup>3</sup>Department of Anatomy and Cell Biology, Osaka Medical College, Takatsuki, Japan

## Correspondence

Masashi Yamamoto, Department of General and Gastroenterological Surgery, Osaka Medical College, 2-7 Daigakumachi, Takatsuki, Osaka 569-8686, Japan.  
Email: sur138@osaka-med.ac.jp

## Abstract

Recently, the feasibility of real-time indocyanine green (ICG) fluorescence imaging-guided complete mesocolic excision in colon cancer surgery has been demonstrated; however, its application to the evaluation of lymphatic flow in widespread lymph node metastasis is uncertain. This study aimed to evaluate lymphatic flow using the real-time ICG fluorescence imaging. A mouse model of subcutaneous inoculation of BJMC3879Luc2 cells, which have been demonstrated to highly metastasize to the lymph nodes, was used as an evaluation model. Tumor growth and lymphatic flow were monitored weekly by bioluminescent imaging and near-infrared (NIR) fluorescence imaging, respectively. After sacrificing the mice, lymph node metastases were evaluated by bioluminescent imaging and histopathology. Lymphatic flows in a model of high lymph node metastasis were evaluated using NIR fluorescence imaging. Pathological metastases of bilateral axillary, femoral, and para-aortic lymph nodes were detected in all inoculated mice (100%: 5/5). Real-time NIR fluorescence imaging showed the primary lymphatic vessels staining through the metastatic lymph nodes as before the inoculation of the cancer cells. Hitherto, it has been considered that lymphatic flow was changed using the bypass pathway due to occlusion of the primary lymphatic vessels. In this presented study, real-time ICG fluorescence imaging showed no changes in lymphatic flow after lymph node metastasis. Our results suggest that real-time ICG fluorescence imaging may have potential for the guidance of colon cancer surgery in cases of widespread lymph node metastasis.

## KEYWORDS

colon cancer, indocyanine green, lymph node metastasis, lymphatic flow, near-infrared fluorescence

**Abbreviations:** BW, body weight; CME, complete mesocolic excision; CVL, central vascular ligation; FBS, fetal bovine serum; H&E, hematoxylin and eosin; ICG, indocyanine green; NIR, near-infrared; PBS, phosphate-buffered saline; ROI, region of interest; RT-ICG-NIR, real-time-indocyanine green-near-infrared.

This is an open access article under the terms of the Creative Commons Attribution-NonCommercial-NoDerivs License, which permits use and distribution in any medium, provided the original work is properly cited, the use is non-commercial and no modifications or adaptations are made.

© 2020 The Authors. *Cancer Science* published by John Wiley & Sons Australia, Ltd on behalf of Japanese Cancer Association.

## 1 | INTRODUCTION

Colorectal cancer is the third most common cancer worldwide, with an estimated 1.4 million new cases per year.<sup>1</sup> Complete mesocolic excision (CME) with central vascular ligation (CVL) is expected to be a novel approach for transverse colon cancer surgery.<sup>2,3</sup> The problematic technical point for the operation of colon cancer located in the hepatic flexure or splenic flexure is that the precise lymphatic dissection is uncertain due to the diversity of lymphatic drainage at this site.<sup>4-7</sup> Based on this anatomical difficulty, laparoscopic surgeries in these areas are not standardized. In many clinical trials, patients with colon cancer in these locations have been excluded due to a lack of standardization of operative procedures.<sup>8-11</sup>

In recent years, several reports have demonstrated the utility and feasibility of visualization of lymphatic flow using indocyanine green (ICG) near-infrared (NIR) fluorescence imaging.<sup>12-14</sup> The concept of this method differs from sentinel lymph node mapping in terms of selective removal of the mesocolon, draining the tumor, and an understanding of the lymphatic flow pattern may help identify the mesocolic excision.<sup>13</sup> Namely, real-time ICG-NIR (RT-ICG-NIR) fluorescence imaging has potential for optimization and individualization of CME without the false-negative results of sentinel lymph nodes.

However, in widespread lymph node metastasis cases, lymphatic vessel obstruction may induce a misinterpretation of the dissection because the lymphatic flow may be bypassed to other lymph nodes.<sup>15</sup> Although RT-ICG-NIR has a latent risk of misinterpretation, there are no studies in cases of advanced lymph node metastasis that have examined the lymphatic flow pattern using this method. To use RT-ICG-NIR fluorescence imaging in clinical practice, the definite lymphatic flow pattern should be determined in cases of widespread metastases. Therefore, in this study, we attempted to elucidate the lymphatic flow pattern using a highly metastatic lymph node mouse model.

## 2 | MATERIALS AND METHODS

### 2.1 | Cell lines and cell culture

The BJMC3879Luc2 is a mammary adenocarcinoma line developed in a BALB/c female upon inoculation of the mouse mammary tumor virus into the inguinal mammary glands.<sup>16-18</sup> The cells were established by Dr Masa-Aki Shibata, our collaborator, in an earlier study.<sup>16</sup> The cells were maintained in RPMI-1640 medium (FUJIFILM Wako Pure Chemical Corporation) supplemented with 10% (v/v) heat-inactivated fetal bovine serum (FBS; Gibco; Thermo Fisher Scientific, Inc), in a 5% CO<sub>2</sub> atmosphere at 37°C.

### 2.2 | Animals

Five 6-week-old female BALB/c nude mice were purchased from Japan SLC, Inc. The mice were housed in plastic cages, with no more

than five mice per cage, on wood chip bedding with free access to water and food and maintained under conditions of controlled temperature ( $21 \pm 2^\circ\text{C}$ ), humidity ( $50 \pm 10\%$ ), and lighting (12 hour-12 hour light-dark cycle).

All mice were held for a 1-week acclimatization period before test initiation. All manipulations and treatments were performed in accordance with procedures outlined in the Guide for the Care and Use of Laboratory Animals of the National Institutes of Health.<sup>19</sup> The study protocol was approved by the Osaka Medical College Animal Care and Use Committee (approval number 2019-118). The body weight (BW) was recorded every 7 days, and the mice were sacrificed after 21 days. On the termination of the study, all mice were euthanized using an isoflurane anesthesia system (Shinanoseisakusho CO., LTD).

### 2.3 | Transplantation method

Under the same sedation conditions,  $5 \times 10^6$  BJMC3879Luc2 cells in 0.3 mL of phosphate-buffered saline (PBS) were inoculated subcutaneously into the right inguinal region of the five BALB/c nude mice using a 27 G needle. Tumor volume was measured once a week and calculated using the formula: length  $\times$  width  $\times$  depth  $\times$  0.5236.<sup>20</sup>

### 2.4 | Fluorescence imaging

While under isoflurane inhalation, 0.1-0.2  $\mu\text{L}$  of ICG solution (Diagnogreen; Daiichi Sankyo Co., Ltd.; 2.5 mg/mL in distilled water) was inoculated subcutaneously into the right inguinal region of the BALB/c nude mice with a 27 G needle. NIR fluorescence images were acquired using a SPY Portable Handheld Imager™ (Stryker). This device consists of a 3-W, 806-nm laser diode, and the system optics spread the laser output over a field of 7.6 cm by 7.6 cm square, at a distance of 30 cm, resulting in a maximal intensity of 30 mW/cm<sup>2</sup>. The unit also contained two charge-coupled device video cameras sensitive to the NIR of the spectrum, each equipped with a different fixed focal length lens and iris. This system included the SPY Mode (NIR fluorescence was displayed in grayscale), the PINPOINT Overlay Mode (a combination of white-light and the NIR fluorescence image, appearing as fluorescent green on top of a high-definition white-light image) as well as the Color-Segmented Fluorescence (CSF) Mode (the NIR fluorescent image was color-scaled, with red representing the highest degree of fluorescence and blue being the least).

### 2.5 | Bioluminescence imaging

The mice were injected intraperitoneally with D-luciferin potassium salt (Wako Pure Chemical Corporation) at 3 mg/mouse. Bioluminescent signals received during the 6-minute acquisition

time were quantified using the IVIS Lumina in vivo imaging system and Living Image Software Version 4.0 (Perkin Elmer). Tumor area was measured using the region of interest (ROI) contour tool.

## 2.6 | Histopathological assessment

At necropsy, tumors and lymph nodes—routinely, the axillary and femoral nodes, as well as those appearing abnormal—were removed and fixed in 10% formaldehyde solution in phosphate buffer. Then, the specimens were processed through paraffin embedding (Naraboury Laboratory Co., Ltd.). All tissues were cut into subsequent 4- $\mu$ m-thick sections and stained with hematoxylin and eosin (H&E) (Muto Pure Chemical Co., Ltd.) for histopathological examination.

## 3 | RESULTS

### 3.1 | Fluorescence imaging of lymphatic flow after injection of ICG

After ICG had been injected into the right inguinal region (Figure 1A-C), lymphatic flow to the right axillary lymph node was detected using

RT-NIR fluorescence imaging in all animals (Figure 1D,E). The lymphatic flow reached the axillary lymph node at 3-5 minutes after the injection.

### 3.2 | Our mouse model was suitable for lymphatic flow investigation

Seven days after the inoculation of the BJMC3879Luc2 cells, all engrafted tumors were observed macroscopically (Figure 2A). Also, bioluminescence of the tumors could be detected by the IVIS imaging system (Figure 2B), and 2 weeks after inoculation of the cells, bioluminescence was identified at the metastatic right axillary lymph node. At 21 days, metastasis of the opposite (left side) axillary lymph node was detected (Figure 2B). Naturally, the bioluminescence of the right femoral region included the metastatic femoral lymph node (Figure 2B). Gradual tumor growth was detected during the observation period by all test methods (Figure 2A-D). No statistically significant weight loss was observed between control and tumor-engrafted mice over a period of 21 days (Figure 2E). These results suggested that this highly metastatic lymph node mouse model is suitable for the investigation of lymphatic flow in a widespread lymphatic metastatic situation.

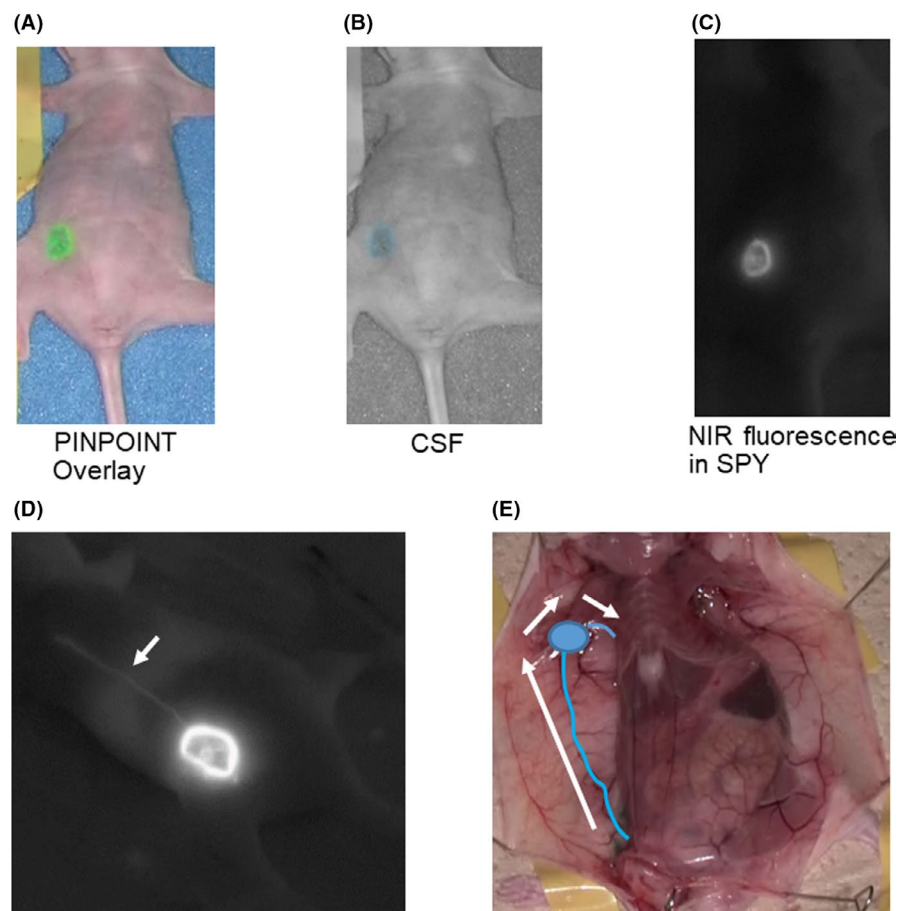


**FIGURE 1** The near-infrared (NIR) fluorescence image of the injection site in the ventral up position after injection of indocyanine green (ICG). The injection site was in the right inguinal region. ICG solution was injected subcutaneously with a 27 G needle under anesthesia. A, PINPOINT Overlay Mode localized the injection site (appeared as fluorescent green). B, Color-Segmented Fluorescence (CSF) Mode identified the areas of high rate and concentration of ICG (appeared as red). Central area was stained pale red. C, NIR fluorescence in SPY Mode identified the same area as in (A) and (B) (appeared as white). D, NIR fluorescence in SPY Mode indicated a lymphatic vessel to the right axillary lymph node filled with ICG (white arrow). E, Schematic drawing showed the primary lymphatic flow through the right axillary lymph node (blue line and white arrow)

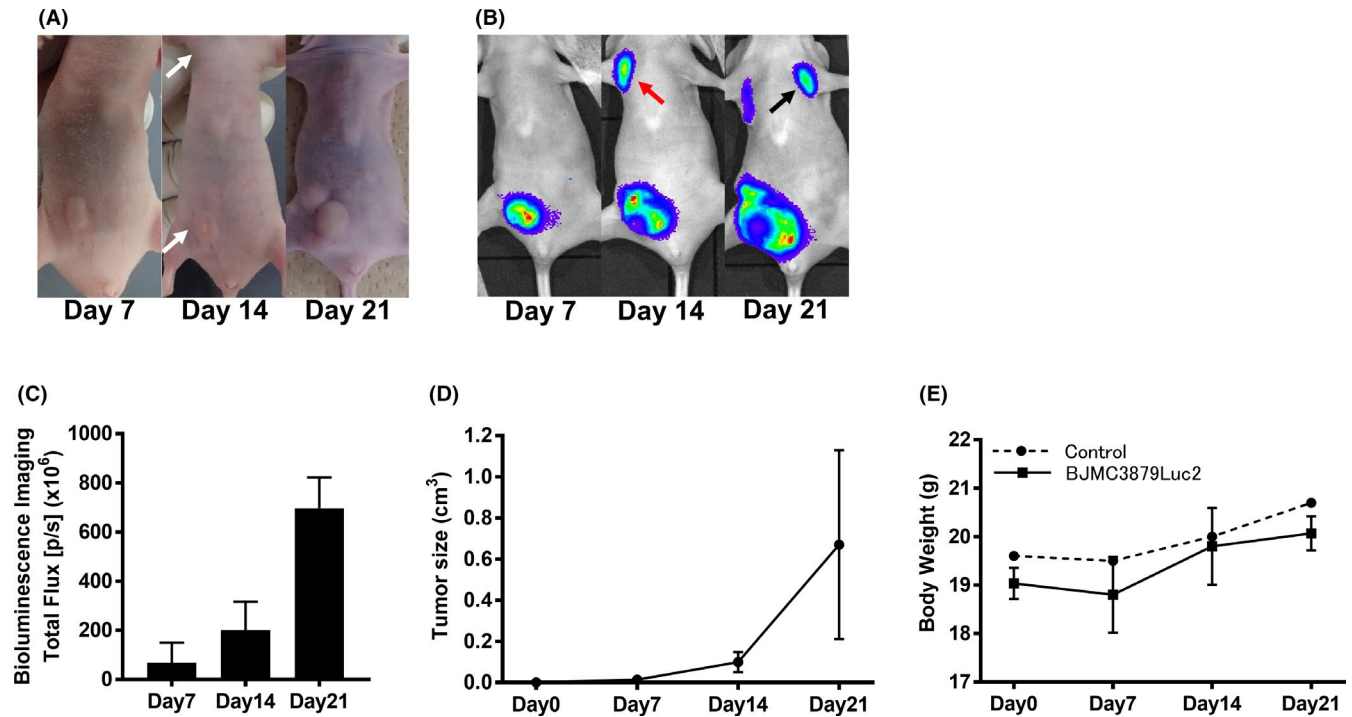


**FIGURE 2** Representative images of tumor growth. The images were measured every 7 d. A, Images of the tumor from the surface of the body. The right axillary and femoral lymph nodes (white arrow) were swollen at 14 d. B, Images from the Xenogen IVIS imaging system. The right axillary region (red arrow) showed a signal at 14 d, while the left axillary region (black arrow) showed a signal at 21 d post inoculation in animal #1. A signal of the right femoral region included the metastatic right femoral lymph node. C, Total photon flux results after 6 min from the luciferin injection. D, Total tumor volumes at 7, 14, and 21 d after inoculation of BJMC3879Luc2 cells. E, The differences in body weight change between control mice and the BJMC3879Luc2 group

### 3.3 | RT-ICG-NIR imaging showed lymphatic flow through the metastatic lymph nodes

Indocyanine green was injected into the right side of the tumor, and lymphatic flow to the right axillary lymph node was detected by RT-ICG-NIR fluorescence imaging in all mice tested. After injection, an incision from suprasternal to the suprapubic region was made, and the metastatic lymph nodes were confirmed macroscopically (Figure 3A). Interestingly, RT-ICG-NIR showed the other lymphatic vessels (ie, right femoral, left axillary, and left femoral lymph nodes; Figure 3B). RT-ICG-NIR showed the primary lymphatic flow stain gradually through the metastatic right axillary lymph node as before the inoculation of the cancer cells (Figure 3C). The whole and cut surface of the right axillary lymph node after sacrificing showed the staining of RT-ICG-NIR (Figure 3D). The H&E staining pathologically also showed metastasis of the lymph nodes (Figure 3E,F). These findings suggested that RT-ICG-NIR fluorescence imaging could show the lymphatic vessels through the metastatic lymph nodes without interruption even in cases of metastatic lymph nodes.

### 3.4 | RT-ICG-NIR showed lymphatic flow by ICG injection around tumor of a large size

To observe the connection between lymphatic drainage and other lymph nodes caused by bulky tumors, we injected ICG around the

local tumor growth of 21-day mice (Figure 4A). RT-ICG-NIR showed several lymphatic flows to the right axillary lymph node, even in the presence of metastatic femoral lymph nodes. Furthermore, the other lymphatic flows to the opposite-side axillary lymph node were observed (Figure 4B). These findings, altogether, suggested that, overall, lymphatic flow was uninterrupted even in the presence of tumors of a large size (Figure 4C).

## 4 | DISCUSSION

This is the first experimental study to evaluate and compare changes in lymphatic flow with highly metastatic lymph nodes in an animal model using RT-ICG-NIR fluorescence imaging. Several studies have demonstrated the oncological outcomes of laparoscopic surgery for transverse and descending colon cancer.<sup>21-23</sup> Colon cancer surgery for hepatic and splenic flexure with CME-CVL correlates with the complex anatomy and necessity for meticulous dissection around a critical structure. We previously showed that the assessment of the variation of the vessels and adjacent structures by preoperative three-dimensional computed tomography simulation may help to overcome these problems.<sup>5,6</sup> Moreover, recently, RT-ICG-NIR has been recognized as a supportive method that determines the appropriate separation line of the mesentery via the identification of central vessels that are

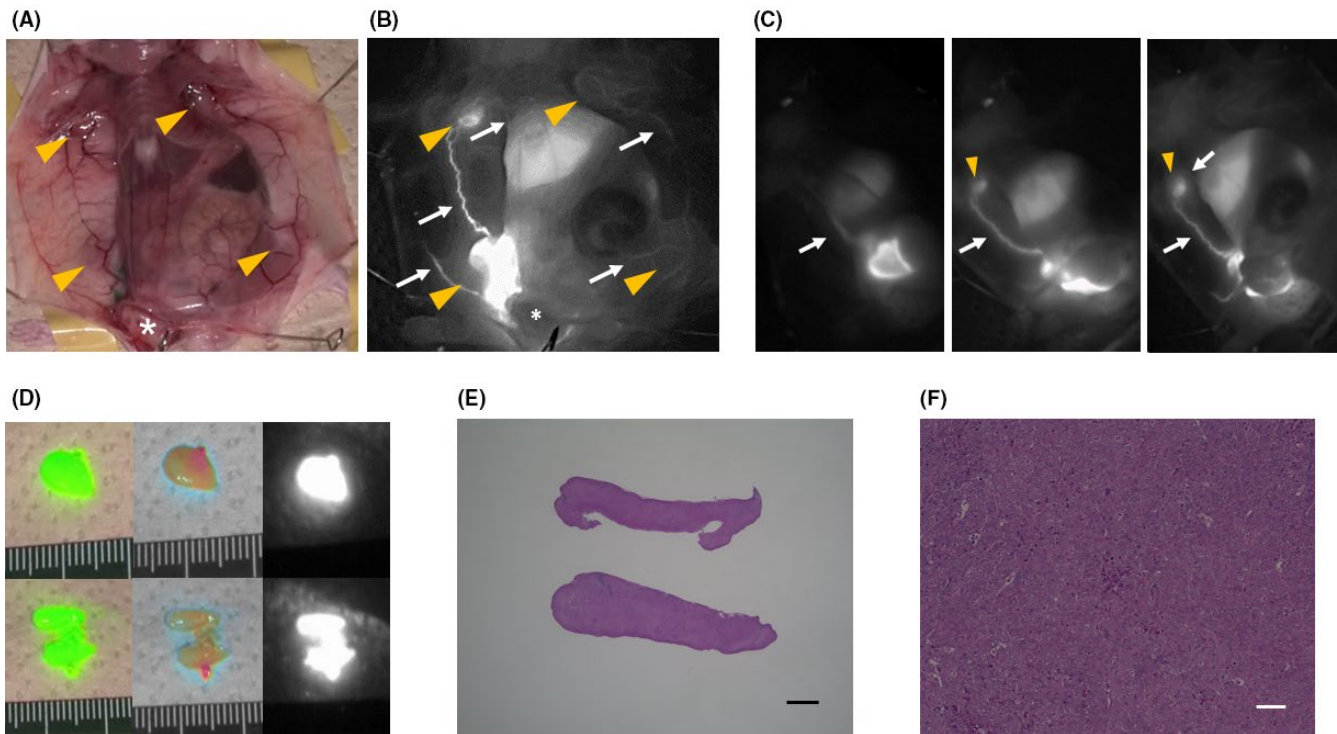


**FIGURE 3** Correlation between macroscopic and histological findings in representative mice. A, In animal #2 placed in the ventral up position, the primary tumor (asterisk) and the lymph nodes showed macroscopic abnormalities at necropsy. Yellow arrowheads indicate axillary and femoral lymph nodes. B, Near-infrared (NIR) fluorescence in SPY Mode showed the primary tumor (asterisk), lymphatic vessels (white arrows), and the lymph nodes (yellow arrowheads). C, Representative continuous images of NIR fluorescence in SPY Mode indicated the primary lymphatic flow through the metastatic right axillary lymph node filled with indocyanine green (ICG). D, The whole (upper pictures) and cut (lower pictures) surface of the right axillary lymph node was stained by ICG. Left pictures, PINPOINT Overlay Mode; middle pictures, Color-Segmented Fluorescence (CSF) Mode; right pictures, NIR fluorescence in SPY Mode. E, Metastasis was histologically confirmed in the right axillary lymph node by hematoxylin and eosin (H&E) stain. Scale bar: 1000  $\mu\text{m}$ . F, Cancer cells were located in the whole of the right axillary lymph node (H&E stain). Scale bar: 50  $\mu\text{m}$

appropriate for dissection.<sup>12-14</sup> On the other hand, widespread lymph node metastases have been observed to induce an obstruction of lymphatic channels, and lymphatic drainage is bypassed to other (nonsentinel) lymph nodes.<sup>15</sup> This phenomenon is a critical issue when using RT-ICG-NIR.

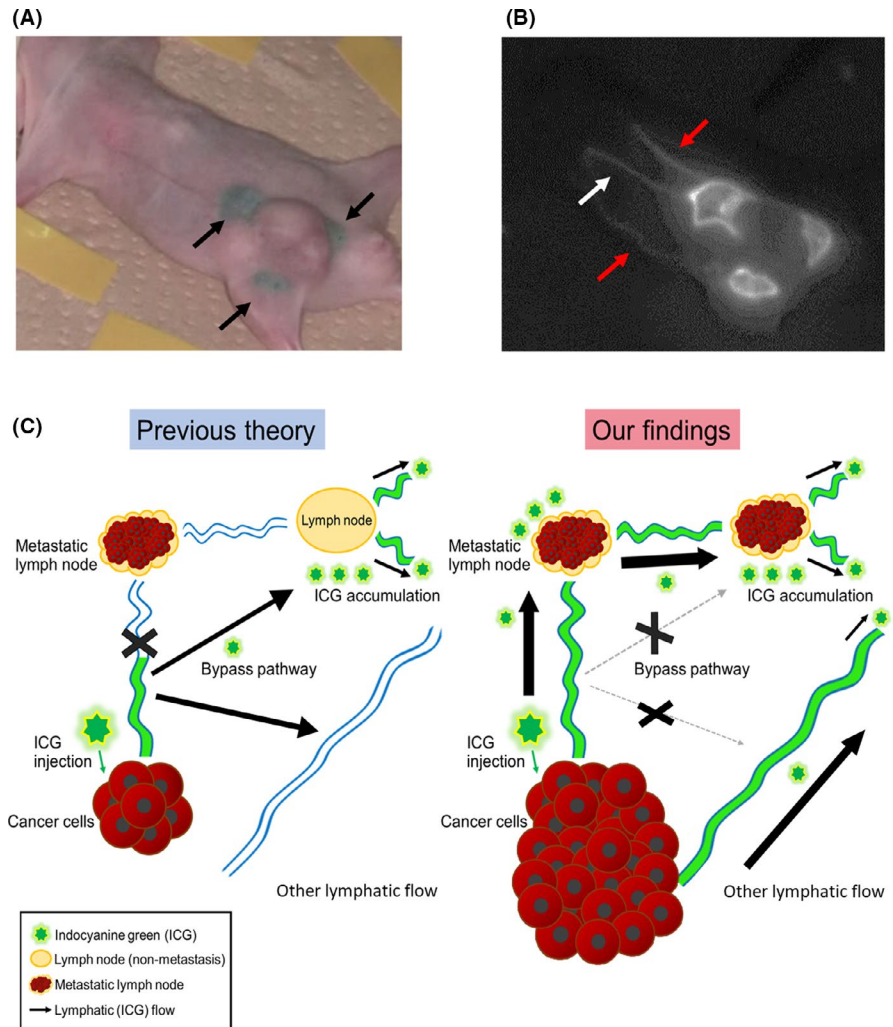
In this study, the lymphatic flow patterns were observed by RT-ICG-NIR in a highly metastatic lymph node mouse model. Lymphatic flow was visualized in all mice before inoculation (Figure 1B). Also, all metastatic lymph nodes (ie, bilateral axillary, femoral, and para-aortic lymph node) were similarly detected by RT-ICG-NIR (Figure 3B-E). Furthermore, RT-ICG-NIR fluorescence imaging showed staining of the lymphatic vessels through the metastatic lymph nodes (Figure 3B). In the present study, we did not observe bypassed lymphatic drainage to other lymph nodes. Although it has been considered that bypassed lymphatic drainage was formed by the obstruction of lymphatic channels by metastases in the lymph nodes,<sup>15</sup> our findings imply that most of the lymphatic vessels are small and create a maze of interlacing vessels together with the lymph nodes (Figure 4C). After injection of ICG around a large tumor, lymphatic flow to the other right axillary lymph node was observed by RT-ICG-NIR (Figure 4A,B). We consider the expanded tumor have several lymphatic flow in this study. These results may

suggest that large tumors have multiple lymphatic drainage vessels in clinical cases. Previously, Norrmen et al proposed a complex lymphatic vascular system,<sup>24</sup> and Nakajima et al detected the lymphatic drainage pathways and connections using the NIR fluorescence image in a lymphedema mouse model.<sup>25</sup> These findings support our consideration. Several reports have also indicated that these phenomena may be called skip lymph node metastasis without bypassed lymphatic flow.<sup>14,26</sup> Probably, more complex lymphatic vessels exist in cases of widespread lymph node metastases.

There are several limitations associated with this study. First, this study was performed using an immune-compromised mouse model. Although lymphatic flow could not detect cases with diverticulitis,<sup>15</sup> an inflammatory change due to immune responses such as fibrosis should be considered in lymphatic vessel obstruction, including metastatic cancer. This study aimed to confirm whether the lymphatic flow pattern could be detected by RT-ICG-NIR fluorescence imaging. Regarding this point, the nude mouse was most suitable because RT-ICG-NIR easily detects the lymphatic flow macroscopically without the use of a unique technique.

In conclusion, our findings suggest that RT-ICG-NIR may have potential for the optimization and/or individualization of CME for laparoscopic hepatic or splenic flexure colon cancer surgery,

**FIGURE 4** The fluorescence image of the lymphatic vessels after injection of indocyanine green (ICG) around the tumor. A, The injection site of ICG was around the primary tumor (black arrows). B, A representative picture of near-infrared (NIR) fluorescence in SPY Mode. Lymphatic flow from the injection site of ICG to the right axillary lymph node was observed (white arrow) through the metastatic femoral lymph nodes. The other lymphatic flows also were observed (red arrows). C, Schematic diagram of our findings. ICG flows through the lymphatic vessels and is used for the detection of metastatic lymph nodes. The left schema shows the previous theory regarding ICG flow in the presence of metastatic lymph nodes. Hitherto, it has been considered that lymphatic flow was changed using the bypass pathway due to occlusion of the primary lymphatic vessels. However, our experiments did not show the bypass pathway under metastatic conditions. Our analyses also showed that ICG flows through the primary lymphatic vessels, even in metastatic lymph nodes. The other lymphatic flow patterns were observed around the expanded tumor (right schema)



with or without lymph node metastasis. Additional clinical studies with a larger population, together with clinical outcomes, are needed to investigate whether it is possible to selectively remove the mesocolon, draining a tumor, by RT-ICG-NIR fluorescence imaging.

#### ACKNOWLEDGMENTS

The authors thank Ms Akiko Miyamoto (in our laboratory), Mr Taka-aki Ishizuka (Division of Research Equipment and Devices at Osaka Medical College), Mr Rintaro Oide, and Ms Akiko Kagotani (Translational Research Program at Osaka Medical College) for their technical support.

#### DISCLOSURE

No potential conflicts of interest were disclosed.

#### ORCID

Masashi Yamamoto  <https://orcid.org/0000-0002-5521-479X>  
 Kohei Taniguchi  <https://orcid.org/0000-0003-0648-1370>  
 Masa-Aki Shibata  <https://orcid.org/0000-0002-3350-7305>  
 Kazumasa Komura  <https://orcid.org/0000-0003-4157-1929>

#### REFERENCES

1. Torre LA, Bray F, Siegel RL, et al. Global cancer statistics, 2012. *CA Cancer J Clin*. 2015;65:87-108.
2. West NP, Hohenberger W, Weber K, et al. Complete mesocolic excision with central vascular ligation produces an oncologically superior specimen compared with standard surgery for carcinoma of the colon. *J Clin Oncol*. 2010;28:272-278.
3. West NP, Kobayashi H, Takahashi K, et al. Understanding optimal colonic cancer surgery: comparison of Japanese D3 resection and European complete mesocolic excision with central vascular ligation. *J Clin Oncol*. 2012;30:1763-1769.
4. Nakagoe T, Sawai T, Tsuji T, et al. Carcinoma of the splenic flexure: multivariate analysis of predictive factors for clinicopathological characteristics and outcome after surgery. *J Gastroenterol*. 2000;35:528-535.
5. Matsuki M, Okuda J, Kanazawa S, et al. Virtual CT colectomy by three-dimensional imaging using multidetector-row CT for laparoscopic colorectal surgery. *Abdom Imaging*. 2005;30:698-708.
6. Kanamoto T, Matsuki M, Okuda J, et al. Preoperative evaluation of local invasion and metastatic lymph nodes of colorectal cancer and mesenteric vascular variations using multidetector-row computed tomography before laparoscopic surgery. *J Comput Assist Tomogr*. 2007;31:831-839.
7. Negoi I, Beuran M, Hostiu S, et al. Surgical anatomy of the superior mesenteric vessels related to colon and pancreatic surgery: a systematic review and meta-analysis. *Sci Rep*. 2018;8:4184.

8. Clinical Outcomes of Surgical Therapy Study Group. Laparoscopic colectomy for cancer is not inferior to open surgery based on 5-year data from the COST study group trial. *Ann Surg.* 2007;246:655-664.
9. The Colon Cancer Laparoscopic or Open Resection Study Group. Survival after laparoscopic surgery versus open surgery for colon cancer: long-term outcome of a randomized clinical trial. *Lancet Oncol.* 2009;10:44-52.
10. Jayne DG, Thorpe HC, Copeland J, et al. Five-year follow-up of the medical research council CLASICC trial of laparoscopically assisted versus open surgery for colorectal cancer. *Br J Surg.* 2010;97:1638-1645.
11. Kitano S, Inomata M, Mizusawa J, et al. Survival outcomes following laparoscopic versus open D3 dissection for stage II or III colon cancer (JCOG0404): a phase 3, randomised controlled trial. *Lancet Gastroenterol Hepatol.* 2017;2:261-268.
12. Nishigori N, Koyama F, Nakagawa T, et al. Visualization of lymph/blood flow in laparoscopic colorectal cancer surgery by ICG fluorescence imaging (Lap-IGFI). *Ann Surg Oncol.* 2016;23(suppl 2):266-274.
13. Watanabe J, Ota M, Suwa Y, et al. Real-time indocyanine green fluorescence imaging-guided complete mesocolic excision in laparoscopic flexural colon cancer surgery. *Dis Colon Rectum.* 2016;59:701-705.
14. Watanabe J, Ota M, Suwa Y, et al. Evaluation of lymph flow patterns in splenic flexural colon cancer using laparoscopic real-time indocyanine green fluorescence imaging. *Int J Colorectal Dis.* 2017;32:201-207.
15. Kelder W, Braat AE, Karrenbeld A, et al. The sentinel node procedure in colon carcinoma: a multi-centre study in The Netherlands. *Int J Colorectal Dis.* 2007;22:1509-1514.
16. Shibata MA, Shibata E, Morimoto J, et al. An immunocompetent murine model of metastatic mammary cancer accessible to bioluminescence imaging. *Anticancer Res.* 2009;29:4389-4395.
17. Shibata MA, Morimoto J, Otsuki Y. Suppression of murine mammary carcinoma growth and metastasis by HSVtk/GCV gene therapy using in vivo electroporation. *Cancer Gene Ther.* 2002;9:16-27.
18. Shibata MA, Morimoto J, Otsuki Y. Lovastatin inhibits tumor growth and lung metastasis in mouse mammary carcinoma model: a p53-independent mitochondrial-mediated apoptotic mechanism. *Carcinogenesis.* 2004;25:1887-1898.
19. Kilkenny C, Browne W, Cuthill IC, et al. Animal Research: reporting in vivo experiments: the ARRIVE guidelines. *Br J Pharmacol.* 2010;160:1544-1579.
20. Gleave M, Tolcher A, Miyake H, et al. Progression to androgen independence is delayed by adjuvant treatment with antisense Bcl-2 oligodeoxynucleotides after Castration in the LNCaP prostate tumor model. *Clin Cancer Res.* 1999;5(10):2891-2898.
21. Yamamoto M, Okuda J, Tanaka K, et al. Clinical outcomes of laparoscopic surgery for advanced transverse and descending colon cancer: a single-center experience. *Surg Endosc.* 2012;26:1566-1572.
22. Athanasiou CD, Robinson J, Yiasemidou M, et al. Laparoscopic vs open approach for transverse colon cancer. A systematic review and meta-analysis of short and long term outcomes. *Int J Surg.* 2017;41:78-85.
23. Yamaguchi S, Tashiro J, Araki R, et al. Laparoscopic versus open resection for transverse and descending colon cancer: short-term and long-term outcomes of a multicentre retrospective study of 1830 patients. *Asian J Endosc Surg.* 2017;10:268-275.
24. Norrmén C, Tammela T, Petrova TV, et al. Biological basis of therapeutic lymphangiogenesis. *Circulation.* 2011;123:1335-1351.
25. Nakajima Y, Asano K, Mukai K, et al. Near-infrared fluorescence imaging directly visualizes lymphatic drainage pathways and connections between superficial and deep lymphatic systems in the mouse hindlimb. *Sci Rep.* 2018;8:7078.
26. Vujik FA, Hilling DE, Mieog JSD, et al. Fluorescent-guided surgery for sentinel lymph node detection in gastric cancer and carcinoembryonic antigen targeted fluorescent-guided surgery in colorectal and pancreatic cancer. *J Surg Oncol.* 2018;118:315-323.

**How to cite this article:** Yamamoto M, Taniguchi K, Tominaga T, et al. Evaluation of lymphatic flow pattern using indocyanine green fluorescence imaging in a highly metastatic mouse model. *Cancer Sci.* 2021;112:774-780. <https://doi.org/10.1111/cas.14766>